# Modeling the Segmental Relaxation Time Distribution of Miscible Polymer Blends: Polyisoprene/Poly(vinylethylene)

**Ralph H. Colby\*,† and Jane E. G. Lipson‡**

*Department of Materials Science and Engineering, Pennsylvania State University, University Park, Pennsylvania 16802, and Department of Chemistry, Dartmouth College, Hanover, New Hampshire 03755*

ABSTRACT: In considering the relaxation of segments in a blend whose components have reasonably disparate glass transition temperatures, local concentration fluctuations and density fluctuations each play a role. The result is a distribution of environments around a given segment in the blend, which translates into a distribution of segmental relaxation times. In this work we focus on concentration fluctuations, making use of a simple lattice model to generate a distribution of environments, which we then translate into a dielectric relaxation spectrum. We analyze experimental data for several polyisoprene/poly(vinylethylene) (PI/PVE) blends and show that, by accounting for the relatively strong composition dependence of the blend glass transition temperature, it is possible to model the dielectric relaxation spectrum by considering concentration fluctuations at the scale of the Kuhn length, which is both composition and temperature independent.

## 1. Introduction

Miscible polymer blends are important in industry because they have the potential to lead to new materials without the expense of new synthesis. Like the metal alloys that preceded them, polymer blends often benefit from synergistic effects that make them more useful than a simple linear combination of properties would anticipate. Dynamics in miscible polymer blends are complicated; the time−temperature superposition principle fails in both linear viscoelasticity[1,2] and dielectric spectroscopy[3−8] measurements, and the connection between these two observations is beginning to be understood.[9,10] Each component in the blend appears to exhibit a distinct temperature dependence in its dynamics. Models that account for this complication incorporate local composition variations, caused by either thermally driven concentration fluctuations[7] or chain connectivity,[11,12] or both.[13,14] Indeed, recent computer simulations indicate that both features are important[15,16] As a result, it is expected that there will be different glass transition temperatures for different local volumes of the sample.

Both explanations for local variations in composition reflect the polymeric nature of the components. Connecting monomers into a chain molecule obviates the possibility of random mixing of the monomers.[17] While mixtures of small molecules have thermally driven concentration fluctuations, they are only important very close to (within 1 K of) the critical temperature. In contrast, for polymer blends the very small entropy of mixing makes the free energy of mixing small, with a weak temperature dependence, causing concentration fluctuation effects to be important in these systems even when the temperature is hundreds of degrees from critical.[18]

In the model of Lodge and McLeish[12] monomer connectivity biases the local composition at the scale of the Kuhn length, where segmental dynamics are be-

lieved to operate, while the environment surrounding a locally connected chain is considered to have the macroscopic blend composition. Concentration fluctuation models[7,13,14] treat the problem differently, linking the scale of the local region controlling segmental dynamics to the cooperative size associated with the glass transition.[19−21] The cooperative size grows as temperature is lowered, becoming significantly larger than the Kuhn length near the glass transition temperature, $T_g$. This growing size effectively diminishes the effects of concentration fluctuations, since large volumes will all have essentially the bulk composition. In contrast, experiments show that the dynamics become more complex as temperature is lowered toward $T_g$. This observation, coupled with the expectation that the Kuhn length sets the natural scale for monomer dynamics,[18] leads us to build a model that accounts both for local connectivity and for concentration fluctuations on the scale of the Kuhn length.

In this work we propose a simple lattice model to determine the probability distribution of effective composition, $P(\phi)$, surrounding a given type of monomer out to a distance of roughly the Kuhn length of flexible chain polymers (~1 nm). Using experimental results for the peak segmental relaxation time as a function of composition and temperature, in conjunction with the predicted $P(\phi)$ distributions, we are able to predict the *distribution* of segmental relaxation times at a given temperature and for a given bulk composition. We then compare our predictions with segmental relaxation distribution results from dielectric spectroscopy of PI/PVE blends[8,22] and discuss the strengths and limitations of our approach.

## 2. Lattice Model for Local Environment

Consider a blend of polyA and polyB occupying the sites of a three-dimensional lattice. There are no vacancies, and each site has $z$ nearest neighbors. We take the probability that any one site of the lattice will be occupied by a segment of A to be $\phi$, the site fraction of

† Pennsylvania State University.
‡ Dartmouth College.

A. Since all lattice sites are filled by polymer, $\phi$ is equivalent to the bulk volume fraction of A in the blend. Similarly, the probability of a site being occupied by a segment of B is $1 - \phi$. Note that these probabilities reflect only the relative amounts in the bulk blend of A and B on the lattice, and are independent of the blend thermodynamics. In other words, we treat polyA and polyB as being randomly mixed on this local scale. It would be relatively straightforward to modify our calculations so as to account both for lattice free volume and blend thermodynamics;[23] we intend to revisit these issues in a future paper.

Suppose that a segment of polyA occupies a randomly chosen lattice site, in what we shall call the zeroth shell. In that case, the first coordination shell (consisting of $z$ lattice sites) must include at least two segments of A due to chain connectivity; we ignore end effects throughout. Each of the remaining $(z - 2)$ sites in the first coordination shell may be occupied by a segment of polyA with probability $\phi_A$ or by a segment of polyB with probability $\phi_B$. In this manner we can determine the overall probability of each of the following scenarios: All $z$ of the neighboring sites could be filled with A segments, or $(z - 1)$ of the sites could be filled with A, one site occupied by B, or $(z - 2)$ of the sites filled with A, two sites occupied by B, and so on, down to the last case which is that only the two bonded sites are filled with A and the remaining $(z - 2)$ nonbonded sites are occupied by B (see Appendix for additional details). We now have a set of overall probabilities, each of which is associated with a particular local volume fraction of A (including the segment of A at the center). In other words, we have generated a distribution of (very) local environments. The situation in which a segment of B occupies the zeroth shell site is strictly analogous. In lattice models of this type the lattice spacing plays the role of one of the characteristic parameters of the component. The value of this parameter is typically determined by fitting the theoretical equation of state to pressure−volume−temperature data. In previous work of this sort on hydrocarbon polymer melts[24] we find that a representative lattice spacing is about 2.5 Å. The arithmetic mean of the PI and PVE Kuhn lengths is 11.1 Å, so the 12.5 Å span represented by considering effects out to the second shell, which is a breadth of five lattice sites, should allow us roughly to capture the effects of concentration fluctuations at the scale of the Kuhn length. The precise choice of lattice spacing is tunable (within reason) but can only adopt a single value for a blend.

To generate the more complicated distribution associated with the second shell, it is necessary to consider the connectivity of the lattice. For instance, some of the sites in the second shell are nearest-neighbor to one site in the first shell, while others are nearest-neighbor to two first shell sites. In the latter case we consider that second shell site to be "controlled" by multiple first shell sites, and because of connectivity constraints, this influences the possible outcomes for occupancy even for the situation considered here in which the intermolecular interactions are relatively weak (and therefore likely do not influence nearest-neighbor occupancy). As an example, consider the three-dimensional simple cubic (sc) lattice, for which $z = 6$. A corresponding two-dimensional example is depicted in Figure 1. A central segment of A will have six nearest neighbors; these constitute the first shell, and we assign two of the six
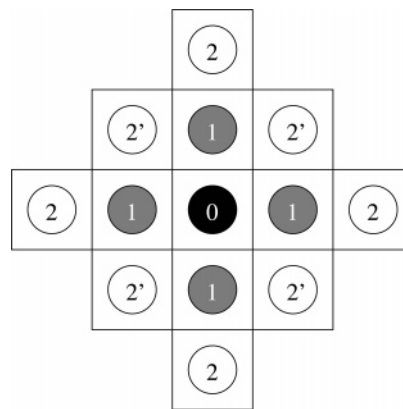


**Figure 1.** Illustration of the zeroth, first, and second shells of the square lattice, filled with monomeric species; the figure therefore does not illustrate any connectivity effects. The black circle occupies the zeroth shell. Gray circles are in the first shell and white circles in the second shell. Second shell sites containing the 2′ are controlled by two of the first shell sites; those containing the 2 are controlled by one first shell site.

to be filled by segments of A which are bonded to the segment in the zeroth shell. Each of the first shell sites therefore has an A in the zeroth shell as one of its six neighbors. The remaining five neighbors of each first shell site are in the second shell; one of these is along the same axis as the zeroth shell; this site is controlled solely by the first shell occupant. However, the remaining four second shell neighbors of the first shell site have shared access; each is, in fact, controlled by two first shell sites. Instead of taking an unmanageable "half" of each of the four sites to be influenced by the first shell site, we assign two of the four sites to be completely controlled by the first shell site. This means that each first shell site completely controls the subsequent filling of three of the 18 second shell sites.

For each scenario of first shell occupancy we can therefore build up occupancy of the second shell, determining the probability of each overall composition using both connectivity and site (volume) fractions as described above. With respect to the former, a little more detail is warranted. If the first shell site in question is occupied by one of the segments of A which was connected to the zeroth shell segment of A, then it must have one connected A in the second shell. On the other hand, if the first shell site is occupied by either a segment of B or an additional (not bonded to the central) A segment, then *two* of its neighboring second shell sites must contain bonded segments of the same type. In this way it is possible to build up two probability distributions associated with an effective local concentration of A (or B) given either an A or a B segment at the center. The resulting distributions will depend on the choice of lattice and on the bulk volume fractions of polyA and polyB but will not depend on the blend thermodynamics or temperature. The example discussed above focused on the simple cubic lattice, for which $z = 6$. Sample calculations are given in the Appendix.

In this paper we work with the simple cubic (sc) lattice although several choices are possible, including tetrahedral ($z = 4$) and body-centered-cubic (bcc, $z = 8$). Note that, given any one of the lattices, for each choice of segment in the zeroth shell there is a minimum self-composition ($\phi_{self}$) out to second shell occupancy due to connectivity constraints. For the sc lattice this will be $\phi_{self} = 5/25$ sites $= 0.2$ (including the segment in the zeroth shell), comparable to the majority of estimates

for $\phi_{self}$ quoted in Lodge and McLeish.[12,25] For the tetrahedral lattice $\phi_{self} = 0.29$, and for the bcc lattice $\phi_{self} = 0.14$.

In this paper we choose the sc lattice in part because it has small enough $z$ that the expressions are not cumbersome (see Appendix), yet $z$ is sufficiently large that there is a reasonable variety of different environments surrounding each monomer, thereby allowing us to obtain a reasonable distribution of segmental relaxation times in each case.[26] This would not be the case for the tetrahedral lattice, for example. The bcc lattice does provide a distribution of environments; however, the $\phi_{self}$ value is low, and the increase in $z$ from 6 (for the sc lattice) to 8 leads to more cumbersome expressions and to distributions which are not qualitatively different than those generated using the sc lattice. Note that our self-concentration ($\phi_{self} = 5/25 = 0.2$ for the sc lattice) only includes the five monomers on the chain that are either the central monomer, directly bonded to the central monomer in the first shell or bonded to those first shell monomers. Therefore, it is a lower bound on the self-concentration, since other parts of the same chain could wind back into the 25-site volume.[15]

We distinguish between $\phi_{self}$ and the composition associated with the maximum in the distribution, which we designate as the effective composition ($\phi_{eff}$). Note also that for any given bulk composition there is a finite probability that all shells will be completely filled by segments of the central type.

In Figure 2a we show the probability distribution going out to the second shell for the case of a segment of type polyA at the center, with bulk probabilities $\phi_A = 0.25$, 0.50, and 0.75. Note that the respective peak maxima are shifted to higher than bulk concentration due to the fact that connectivity ($\phi_{self}$) enriches the local concentration. In Figure 2b the contributions to the overall probability distribution from the various ways of filling the first shell are shown for a bulk composition of $\phi_A = 0.70$. The enrichment of A (and hence the depletion of B) relative to the bulk probabilities is illustrated in Figure 3. The dashed line represents the bulk composition, the filled circles show the composition associated with the distribution's maximum, and the solid line gives the average composition, which is obtained for each value of $\phi_A$ (bulk), by summing the product $\phi_{A,eff} P(\phi_{A,eff})$ over the compositions in the distribution. A feature of the lattice distribution for the sc lattice is that at low ($\phi_A < 0.2$) or high ($\phi_A > 0.8$) bulk compositions the distributions become mildly bimodal, with the appearance of a smaller, local maximum. The open symbols give the composition associated with this local maximum in these limits. This feature disappears when the coordination number increases, for example, in the case of the bcc lattice. The local enrichment in the component occupying the zeroth shell is qualitatively similar to the effective composition, $\phi_{eff}$, defined by Lodge and McLeish, [12] $\phi_{eff} = \phi_{self} + \phi(1 - \phi_{self})$. Indeed, what is shown in Figure 3 as the average composition (solid line) is indistinguishable from the Lodge and McLeish mean-field result. Recall that for the sc lattice ($z = 6$) $\phi_{self} = 5/25 = 0.2$. The effective local concentration distributions (having maxima given by the filled symbols) that we obtain are then used to calculate the local relaxation spectrum via two possible routes, as described in the next section.
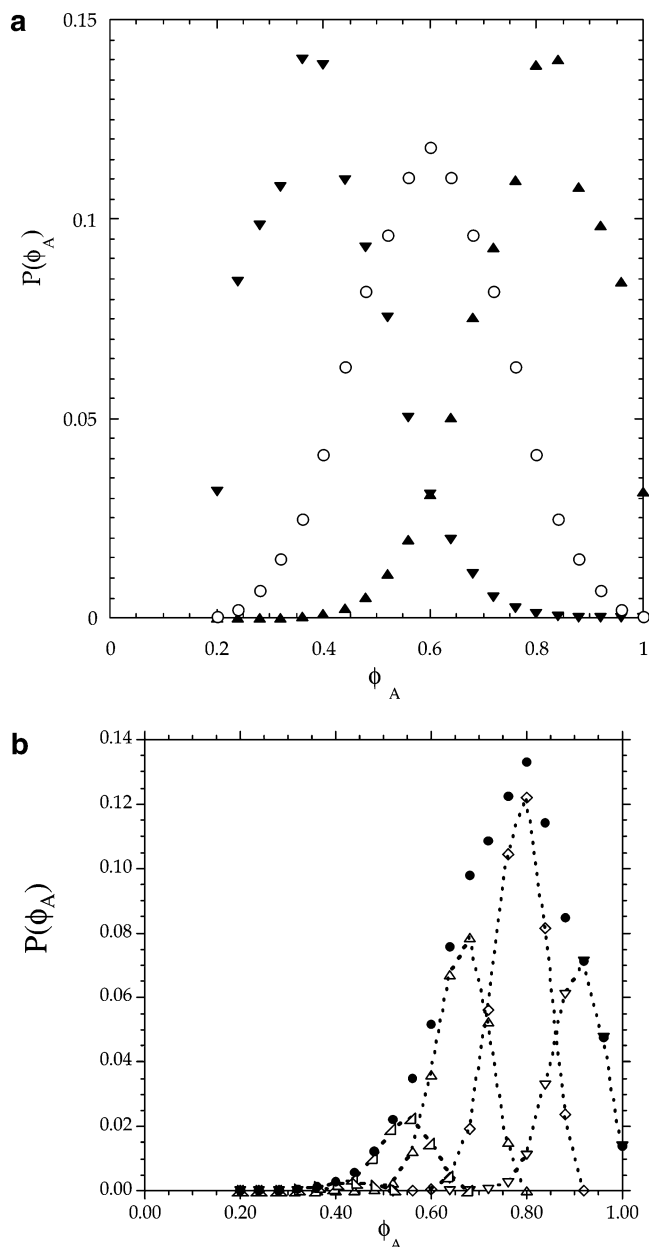


**Figure 2.** Probability distributions for an A-monomer in the zeroth shell being part of a region (through the second shell) with effective volume fraction $\phi$. (a) Probability for the sc lattice ($z = 6$) for three bulk blend compositions: 25% A are filled inverted triangles (with peak at $\phi_A = 0.36$); 50% A are open circles (with peak at $\phi_A = 0.6$); 75% A are filled triangles (with peak at $\phi_A = 0.84$). (b) Probabilities for the sc lattice ($z = 6$) filled to the second shell with bulk composition $\phi = 0.7$ and an A-monomer in the zeroth shell. The contributions from four of the possible first shell contributions are shown, right to left: All 6 A, point-down triangles; 5 A and 1 B, diamonds; 4 A and 2 B, point-up triangles; 3 A and 3 B, right-angle triangles. The black circles show the sum using all possible first shell contributions. Note that the highest three concentrations have open inverted triangles superimposed on filled circles.

## 3. Relaxation Time Distribution

For each component of an experimental blend at any given temperature there is a unique one-to-one mapping between local composition and relaxation time. To generate a predicted relaxation spectrum, it is necessary to choose an approximation for this mapping; we describe two such approximations below.
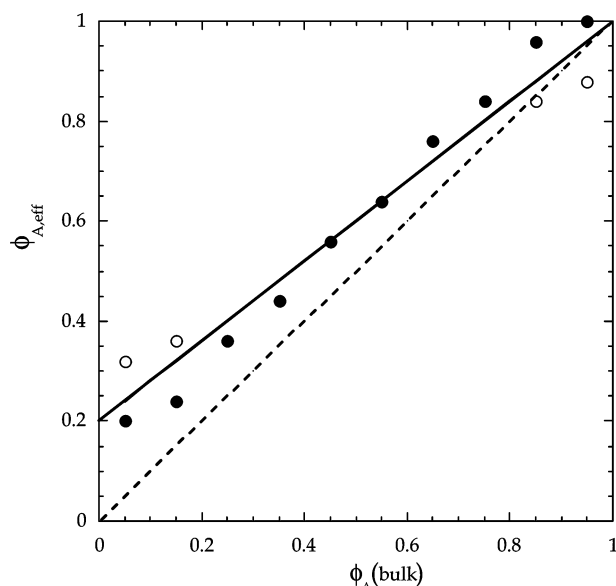
**Figure 3.** Illustration of the local enrichment in A at the scale of the Kuhn length due to segments connected to the A-segment in the zeroth shell. The dashed line represents the bulk concentration; the filled circles represent the global maximum in the composition distribution predicted by the sc lattice model. The open circles represent a second, local maximum where the composition distributions become bimodal. The solid line gives $\phi_A$ (average) predicted by the lattice model (see text for how this is obtained).

**The WLF Route.** The first route involves making use of the Williams–Landel–Ferry (WLF) equation[27]

$$\log\left(\frac{\tau}{\tau_g}\right) = -C_1^g\left[\frac{T - T_g}{T - T_\infty}\right] \quad (1)$$

where $\tau$ is the relaxation time at temperature $T$, and $\tau_g$ is that at the glass transition temperature, $T_g$. $C_1^g$ is a constant referenced to the glass transition temperature. The Vogel temperature $T_\infty$ is where the relaxation time (or viscosity) of the equilibrium liquid diverges. Use of the WLF equation for a single component involves fitting the temperature dependence of the relaxation time in order to obtain values for the three material-specific parameters: $\tau_g$, $C_1^g$, and $T_\infty = T_g - C_2^g$, with $T_g$ as the reference temperature. For each component in a multicomponent system, all of these parameters may be expressed as functions of composition. However, in practice, it is necessary that only two of them have composition dependence, and the choice of the two is open to question. Here we take $\tau_g$ and $C_1^g$ to have their pure component values and fit for $T_g$ and $T_\infty$. At each bulk blend composition we take the reference temperature $T_g$ to be that at which the segmental relaxation time of the particular component in the blend is equal to the segmental relaxation time of the pure component at its own glass transition temperature. $T_\infty$ is then obtained by fitting the temperature dependence of the segmental time associated with the peak maximum for each blend composition. Therefore, for each blend component we require the peak segmental relaxation time data as a function of composition and temperature. For PI/PVE we will use the NMR data of Chung et al.[11] and the dielectric relaxation data of of Alegria et al.[8] At all compositions eq 1, with $\tau_g$ and $C_1^g$ fixed to the pure component values, gives a good description of the temperature dependence of that component's relaxation
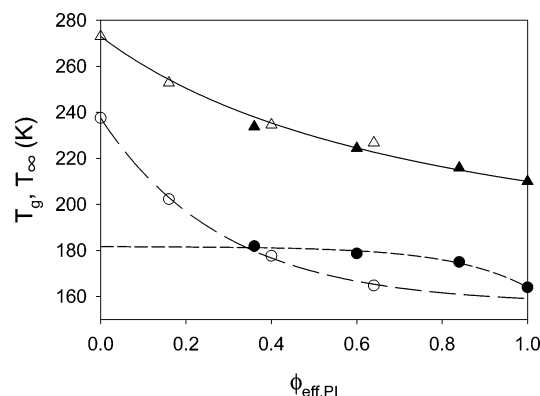


**Figure 4.** Dependence of the glass transition temperature (triangles) and the Vogel temperature (circles) on effective volume fraction of PI, for PI (filled symbols) and PVE (open symbols) in their pure states and their blends, calculated from experimental data by fitting to eq 1. The solid curve is eq 2, and the dashed curves are eqs 3 and 4.

**Table 1. Pure Component WLF Parameters[29]**

| polymer | $\tau_g$ (s) | $C_1^g$ | $T_g$ (K) | $T_\infty$ (K) |
|---------|--------------|---------|-----------|----------------|
| PI | 2.42 | 13.2 | 210.0 | 164.0 |
| PVE | 0.83 | 11.8 | 273.0 | 237.6 |

time in the blend. In Figure 4 we show the results of these fitting procedures for PI/PVE, using pure component data as well as results for bulk composition PI of 25%, 50%, and 75%. Note that the fit parameters $T_g$ and $T_\infty$ are plotted against the *effective* volume fraction of PI. The filled/open triangles represent the $T_g$ results for PI/PVE. The line is a second-order polynomial best fit of the combined two-component system, given by the DiMarzio[28] form

$$T_g = \frac{\phi_{\text{eff,PI}}T_{g,\text{PI}} + 0.45(1 - \phi_{\text{eff,PI}})T_{g,\text{PVE}}}{\phi_{\text{eff,PI}} + 0.45(1 - \phi_{\text{eff,PI}})} \quad (2)$$

where 0.45 was used as a fitting parameter. It is striking that both components show the *same dependence* of $T_g$ on effective local composition, particularly since they have significantly different $\tau_g$ values (see Table 1). It is clear that the effective composition dependence of $T_g$ is considerably stronger than predicted by the Fox equation. Furthermore, the two points that are furthest from eq 2 are PI in a 25% PI blend ($\phi_{\text{eff,PI}} = 0.36$) and PVE in a 75% PI blend ($\phi_{\text{eff,PI}} = 0.64$). The former has too low a PI composition to resolve the PI relaxation in dielectric spectroscopy and hence relies exclusively on NMR data at five temperatures from ref 11. The latter has too low a PVE composition to accurately resolve the PVE relaxation in dielectric spectroscopy. Hence, these two points are the least precise of all the data in Figure 4.

The filled/open circles show the $T_\infty$ results for PI/PVE; here it was not possible to capture the behavior of both components using a single fit. In each case the data indicate a single-exponential decay from the pure component value, such that a saturation effect is observed when the blend becomes "rich enough" in the second component. The fit results are shown as dashed lines in Figure 4, given by

$$T_\infty = 237.6 - 81.0\left[1 - \exp\left(\frac{-\phi_{\text{eff,PI}}}{0.287}\right)\right] \quad \text{(PVE)} \quad (3)$$

$$T_\infty = 164.0 + 17.7\left[1 - \exp\left(\frac{-(1 - \phi_{\text{eff,PI}})}{0.179}\right)\right] \quad (\text{PI}) \quad (4)$$

In looking at Figure 4, we observe an interesting limiting behavior experienced by each component's Vogel temperature at intermediate compositions, whereby the effect of adding a second component saturates well before the first component becomes dilute. This observation should be testable by acquiring data for more dilute compositions of PI/PVE blends, which are slowly becoming available.[30,31]

**The Dynamic Scaling Route.** An alternate route to describing the temperature and composition dependence of the relaxation times is afforded by the dynamic scaling model.[32–34] Like the WLF equation, this description predicts a divergence in the relaxation time (or viscosity) of the equilibrium liquid upon cooling to a temperature $T_c$, *below* $T_g$, as given by

$$\tau = \tau_0\left(\frac{T - T_c}{T_c}\right)^{-9} \quad (5)$$

This form assumes that the polymers are in the fragile limit, wherein $T_c$ is not far (roughly 10–20 K) below $T_g$, making the temperature dependence of relaxation time dominated by the divergence of eq 5 as opposed to the thermally activated process of eq 23 in ref 32. For the case of a single component, use of eq 5 to fit the temperature dependence of the relaxation time yields two constants: $T_c$, the temperature at which the relaxation time diverges, and $\tau_0$, the relaxation time of the liquid at a temperature equal to $2T_c$. The pure component values of these parameters are listed in Table 2. For a blend, the same procedure is used for each composition, and the result is expected to be a set of composition-dependent $T_c$ and $\tau_0$ values. In practice, we find that the $\tau_0$ values for the low-$T_g$ blend component are composition independent. For PI we therefore fix $\tau_0$ to its pure component value and utilize $T_c$ as the sole parameter in fitting the temperature dependence of the PI segmental relaxation times in the blend. For the high-$T_g$ component, PVE, we find the following dependence of $\tau_0$ on the effective local composition of PI

$$\log\left(\frac{\tau_0(\phi_{\text{eff,PI}})}{\tau_0(0)}\right) = 3.275\left[1 - \exp\left(\frac{-\phi_{\text{eff,PI}}}{0.218}\right)\right] \quad (6)$$

The remaining parameter is $T_c$; Figure 5 illustrates the dependence of $T_c$ on effective local composition for each of the two components. As observed with $T_g$ in Figure 4, we find the two blend components have the same dependence of $T_c$ on effective local composition. A fit to this dependence yields the following relationship shown as the solid curve in Figure 5. We note that there

$$T_c = 264.2 - 67.9\left[1 - \exp\left(\frac{-\phi_{\text{eff,PI}}}{0.397}\right)\right] \quad (7)$$

shown as the solid curve in Figure 5. We note that there is a stronger composition dependence of the $T_c$ values than predicted by the Fox equation.

Of the two approaches we have described, the more commonly used method is the WLF route. On the other hand, this method requires fitting to three equations (eqs 2–4) compared to the two needed for dynamic scaling (eqs 6 and 7). In particular, the observation that
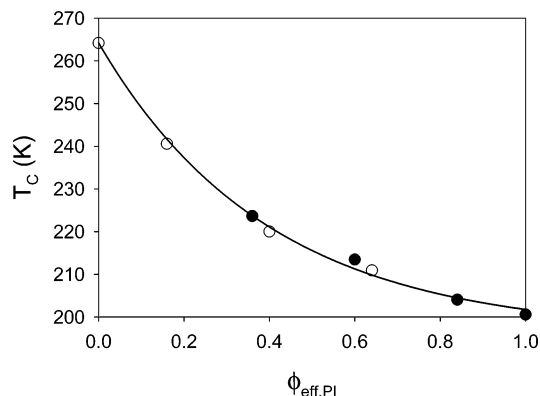


**Figure 5.** Dependence of the critical temperature on effective volume fraction of PI, for PI (filled symbols) and PVE (open symbols) in their pure states and their blends, calculated from experimental data by fitting to eq 5. The solid curve is eq 7.

**Table 2. Pure Component Dynamic Scaling Parameters, Based on Dielectric Data for PI[14] and PVE[8]**

| polymer | $\tau_0 \times 10^{12}$ (s) | $T_c$ (K) |
|---------|------------------------------|-----------|
| PI      | 6.2                          | 200.6     |
| PVE     | 0.062                        | 264.2     |

one equation describes the critical temperature of *both* components in the dynamic scaling route, compared with separate equations for each blend component in the WLF route, makes the dynamic scaling route simpler and more robust. Furthermore, while the two methods do lead to qualitatively similar predictions, the dynamic scaling method is more attractive for our purposes simply because it appears to yield a more accurate description of the segmental relaxation time distributions, and that is the approach we take in what follows.

## 4. Results and Discussion

In section 2 we outlined how to generate the distribution of effective compositions surrounding a central monomer on the scale of the Kuhn length, given the bulk composition, and in section 3 we discussed two descriptions of the temperature dependence of relaxation for different local compositions. The parameters used in these descriptions either are constants or are functions only of effective local composition. The next step is to combine these calculations, using the fitted dependences on $\phi_{\text{eff,PI}}$ for purposes of interpolation, to generate a predicted relaxation spectrum to compare with experiment.

The methods described in the previous section yield a set of values for the characteristic parameters, associated with the set of local compositions in the distribution. At any given temperature and effective composition of interest, application of either eqs 1–4 or eqs 5–7 will determine the relaxation time for that composition/temperature. In this way a relaxation time spectrum for each type of segment may be generated for any set of experimental conditions. The lattice model with $z = 6$ has 21 effective compositions spanning the range from $\phi_{\text{self}} = 0.2$ to the pure component ($\phi_{\text{eff},i} = 0.20$, 0.24, 0.28, ...., 0.96, 1), and these yield the composition distribution. Each composition in the distribution is assumed to relax as a single exponential (Debye relaxation) with a relaxation time that is assigned using eqs 5–7. The dielectric loss $\epsilon''$ arising from each component
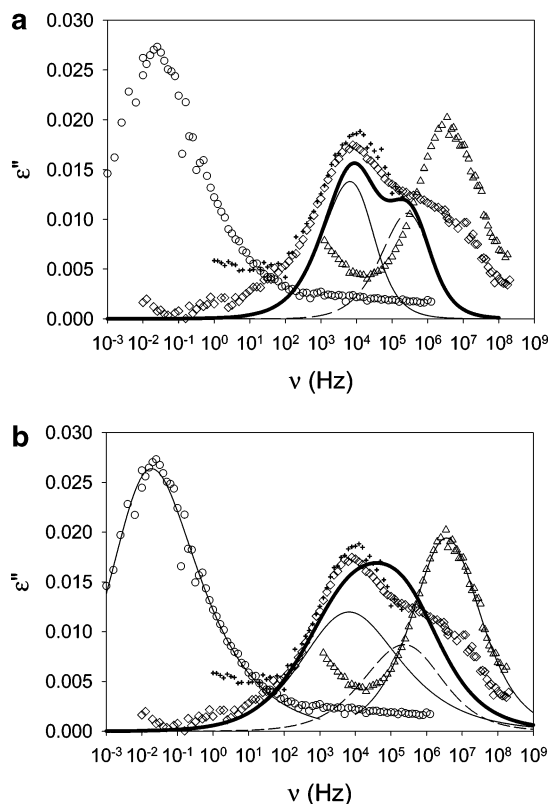
**Figure 6.** Frequency dependence of dielectric loss for PI (triangles), PVE (circles), and a $\phi_{PI} = 0.5$ blend (diamonds, 1999 data; crosses, 1994 data) at $T = 270$ K. All data are from Arbe et al.[22] Predictions from the sc lattice model using the dynamic scaling route are shown for regions surrounding PVE monomers (thin curve), regions surrounding PI monomers (dashed curve), and their sum (thick curve) (a) assigning a Debye relaxation to each environment via eq 8 and (b) assigning a Havriliac−Negami relaxation to each environment via eqs 9−11. Part (b) also shows Havriliac−Negami fits to the pure component polymers as solid curves.

is then calculated as

$$\epsilon''(\omega) = A\phi \sum_{i=1}^{21} P_i \frac{\omega\tau_i}{1 + (\omega\tau_i)^2} \tag{8}$$

where $\omega = 2\pi\nu$ is the angular frequency (in rad/s, $\nu$ is the frequency in Hz), $A$ is a scale factor proportional to the polarizability of the component, $\phi$ is the bulk volume fraction of that component in the blend, and $P_i$ and $\tau_i$ are the probabilities and relaxation times of the 21 discrete local compositions that can surround a monomer of that blend component.

Figure 6a shows the segmental relaxation spectra in the form of dielectric loss data (symbols) at 270 K for pure PI, pure PVE, and a 50% (by volume fraction) blend. This temperature is 3 K below the $T_g$ for pure PVE and 43 K above the experimental blend $T_g$ (the midpoint of the DSC transition). Also shown are the dynamic scaling model predictions (thin line PVE; dashed line PI) for the contribution from each component in the blend as well as their summed contribution (thick line). $A_{PI} = 0.058$ and $A_{PVE} = 0.080$ were chosen to make the heights of the component predictions in the 50% blend half of the pure component experimental peak heights. Note that the small difference between model and experiment for the peak relaxation times reflects the errors introduced in fitting the temperature

and local composition dependences of these times in order to determine values of the characteristic parameters. The predictive power of the model should therefore be judged by its ability to produce a relaxation spectrum having a width and shape that agrees well with experiment. In this context, it is useful to remember that the predicted distributions in Figure 6a reflect only composition, and not density, fluctuations. Therefore, we cannot use this approach to generate relaxation distributions for the *pure* components.

The blend prediction in Figure 6a (thick line) is the sum of the predictions for each of the blend components. Those component predictions comprise 21 discrete points, corresponding to the relaxation times assigned to the 21 discrete local compositions spanning between $\phi_{self}$ (= 0.2 for the sc lattice) and complete filling out to the second shell of the pure component in question (the probability of which is given by our model calculations, see Appendix). Despite this broad range of local compositions, the predicted $\epsilon''(\nu)$ in Figure 6a is too narrow compared with the experimental data because we have not included density fluctuations in our predictions. Consequently, the highest frequency in our predicted $\epsilon''(\nu)$ for the blend is of order $10^7$ Hz, the peak of the pure PI relaxation. Density fluctuations broaden the pure component $\epsilon''(\nu)$, and these effects would need to be included in the blend predictions to obtain quantitative agreement with experiment. However, overall comparison of our model prediction with experimental data in Figure 6a shows that we do capture the bimodal nature of the distribution using Debye relaxations for each composition in the distribution surrounding each type of monomer (eq 8).

An empirical method to include the effects of density fluctuations is to use the Havriliak−Negami function[35]

$$\frac{\epsilon''_{HN}(\omega)}{\Delta\epsilon} = \left[1 + 2(\omega\tau_{HN})^\alpha \cos\left(\frac{\pi\alpha}{2}\right) + (\omega\tau_{HN})^{2\alpha}\right]^{-\gamma/2} \times$$
$$\sin\left(\gamma \tan^{-1}\left[\frac{\sin(\pi\alpha/2)}{(\omega\tau_{HN})^{-\alpha} + \cos(\pi\alpha/2)}\right]\right) \tag{9}$$

to fit the pure component dielectric loss and then assign this same broadened distribution to each composition in the distribution surrounding each type of monomer. $\alpha$ and $\gamma$ are parameters, $\Delta\epsilon$ is the dielectric increment, and $\tau_{HN}$ is the Havriliak−Negami relaxation time, related to the time $\tau$ associated with the peak of the relaxation distribution as[36]

$$\tau_{HN} = \tau \left[\tan\left(\frac{\pi}{2(\gamma + 1)}\right)\right]^{1/\alpha} \tag{10}$$

Equation 9 was fit to the experimental data of Arbe et al.[22] for pure PI and pure PVE at 270 K, shown as the thin solid curves in Figure 6b, and resulting in the parameters $\alpha = 0.603$, $\gamma = 1.03$, $\Delta\epsilon = 0.0750$ for PI and $\alpha = 0.577$, $\gamma = 0.595$, $\Delta\epsilon = 0.133$ for PVE. The dielectric loss contributed by each component in the blend is then calculated from the distribution of environments surrounding that component's monomers (reflected in the $P_i$) as

$$\epsilon''(\omega) = \phi \sum_{i=1}^{21} P_i \epsilon''_{HN,i}(\omega) \tag{11}$$

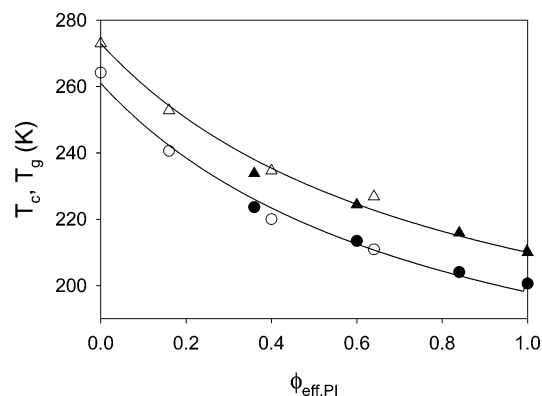where the $\epsilon''_{HN,i}$ are calculated from eqs 9 and 10 using
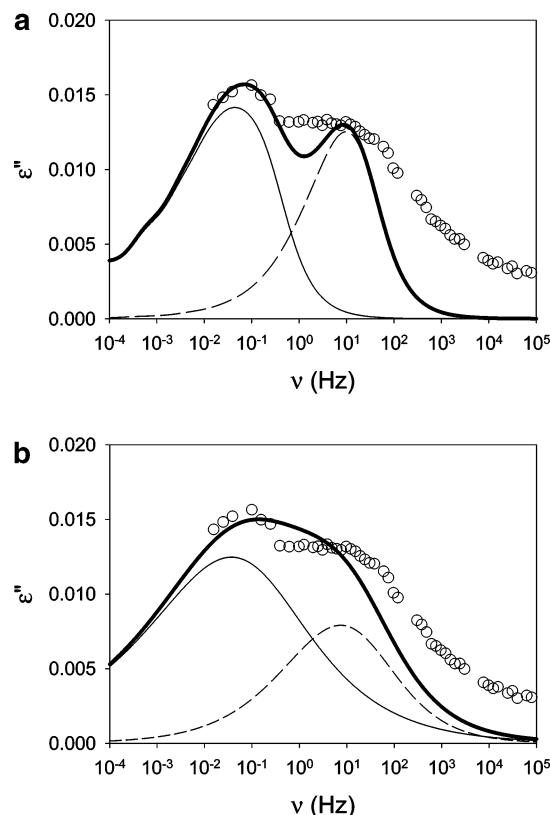
**Figure 7.** Frequency dependence of dielectric loss for a $\phi_{PI} = 0.75$ blend at $T = 223$ K (open circles) from Alegria et al.[8] Predictions from the sc lattice model using the dynamic scaling route are shown for regions surrounding a PVE monomer (thin curve), regions surrounding a PI monomer (dashed curve), and their sum (thick curve) (a) assigning a Debye relaxation to each environment via eq 8 and (b) assigning a Havriliac−Negami relaxation to each environment via eqs 9−11.



**Figure 8.** Comparison of the effective composition dependence of glass transition temperature (triangles) and critical temperature (circles) for PI (filled symbols) and PVE (open symbols) in their pure states and their blends. Solid curves are eq 2, and the same equation shifted downward by 12 K.

the $\tau_i$ values assigned to each local composition by dynamic scaling (eqs 5−7). The resulting predictions for the PI blend component (dashed curve), PVE blend component (solid curve), and their sum (thick curve) are compared with experimental data in Figure 6b. It is clear that the width of the predicted segmental distribution is more consistent with the data when density fluctuations are included using the empirical Havriliak−Negami description. The dielectric increments of the pure components (effectively multiplied by $\phi = 0.5$ for each blend component via eq 11) give reasonable predictions for the $\phi = 0.5$ blend in Figure 6b, although some of the features of the dielectric loss are smeared by the empirical broadening (compare parts a and b of Figure 6).

Figure 7 presents results for a 75% PI/25% PVE blend at a temperature of 223 K, which is 50 K below the $T_g$ of PVE and only 8 K above the DSC blend $T_g$. This represents a more stringent test of our model because the sensitivity of relaxation to composition fluctuations is increased as the experimental temperature is lowered toward the blend glass transition. This case is also interesting in the sense that it has been observed by Kant et al.[29] that in order for the Lodge/McLeish model to work as the experimental temperature approaches the blend $T_g$, the effective volume relevant to the segmental dynamic motion needs to increase. Our model assumes a fixed effective volume that only includes contributions through the second coordination shell, and inspection of Figure 7 suggests that our simple model

captures the peak broadening just as effectively near the blend $T_g$ as it does at higher temperatures.

Figure 7a compares experimental data of Alegria et al.[8] with the blend predictions based on a Debye relaxation for each environment using eq 8. The scale factors ($A_{PI} = 0.053$ and $A_{PVE} = 0.28$ in eq 8) needed in Figure 7a differ from those used in Figure 6a. The scale factor used for PI is likely within experimental uncertainty of that used in Figure 6a ($A_{PI} = 0.058$); however, the scale factor used for PVE is a factor of 3.5 larger than that used in Figure 6a. While dielectric increments (relaxation strengths) do change with temperature and could change with composition, such a large change would be surprising. On the basis of the pure component peak height of 0.028 for PVE in Figure 6, one might naively expect that the peak height of PVE in a 25% PVE blend would be 0.007. The actual peak height for PVE in the 25% PVE blend in Figure 7 is twice this value and comparable to the PVE peak in the 50% PVE blend of Figure 6.

Figure 7b shows the blend predictions based on the Havriliak−Negami description of eqs 9−11. As observed in Figure 6, the width of the predicted dielectric loss distribution for the blend is improved by including the empirical broadening, at the expense of losing some of the features. Similar to the scale factors used in Figure 7a, the dielectric increments used for the blend predictions in Figure 7b were adjusted to give better descriptions of the experimental dielectric loss ($\Delta\epsilon = 0.150$ for PI compared with $\Delta\epsilon = 0.0750$ for pure PI and used for the PI component blend prediction in Figure 6b; $\Delta\epsilon = 0.372$ for PVE compared with $\Delta\epsilon = 0.133$ for pure PVE and used for the PVE component blend prediction in Figure 6b). The origins of these adjusted dielectric increments (Figure 7b) and scale factors (Figure 7a) are not understood; one possible explanation would be a different microstructure of the chains used in the blend shown in Figure 7.

In looking at Figures 4 and 5, it is apparent that the effective composition dependences of both $T_c$ (the divergence temperature in dynamic scaling) and $T_g$ (the temperature at which each blend component has the same relaxation time as the pure component at its $T_g$) appear to be very similar. This impression is supported by Figure 8, in which the composition dependences of these two temperatures are compared directly. The solid line associated with the $T_g$ points is shown in Figure 4 (eq 2). In Figure 8 this line appears again, shifted down

**Table 3. Comparison of the Difference between $T_g$ and $T_c$ As Obtained Separately, Using Eqs 1 and 5 and Together Using Eq 12**

| segment | $\phi_{bulk}$ | $\phi_{eff}$ | $T_c$ (K) eq 5 | $T_g$ (K) eq 1 | $T_g - T_c$ (K) eqs 1 and 5 | $T_c$ (K) eq 12 | $T_g$ (K) eq 12 | $T_g - T_c$ (K) eq 12 |
|---------|---------|--------|-----------|-----------|-------------------|------------|-----------|------------------|
| PI | 0.75 | 0.84 | 207.4 | 216.7 | 9.3 | 204.1 | 215.9 | 11.8 |
| PVE | 0.75 | 0.64 | 209.7 | 227.4 | 17.7 | 210.9 | 226.8 | 15.9 |
| PI | 0.50 | 0.60 | 215.0 | 225.4 | 10.4 | 213.5 | 224.4 | 10.9 |
| PVE | 0.50 | 0.40 | 218.8 | 235.0 | 16.2 | 220.0 | 234.6 | 14.6 |
| PI | 0.25 | 0.36 | 221.2 | 234.2 | 13.1 | 223.7 | 233.8 | 10.1 |
| PVE | 0.25 | 0.16 | 238.7 | 253.1 | 14.4 | 240.6 | 252.8 | 12.2 |
| average | | | | | $13.5 \pm 3$ | | | $12.5 \pm 2$ |

by 12 K, and appears to do essentially as well at capturing the composition dependence of $T_c$, as it did for $T_g$. If $T_g - T_c$ is indeed constant, it suggests a simplified route for connecting the concentration distribution to the dielectric relaxation spectrum. For each component in the blend, consider the ratio between the relaxation time at temperature $T$ and that at $T_g$. Using eq 5, we obtain

$$\tau = \tau_g \left( \frac{T - T_c}{T_g - T_c} \right)^{-9} \tag{12}$$

Recall that $\tau_g$ is the relaxation time of the segment at the glass transition temperature of the *pure* component, and $T_g$ is defined as the temperature at which the segment in the blend has a relaxation time of $\tau_g$. We refit the dielectric and NMR data using eq 12 so as to obtain optimized values of $T_g$ and $T_c$ for each component. The values for each of the two temperatures are listed in Table 3 and compared with the values obtained previously from applying eq 1 (for $T_g$) and eq 5 (for $T_c$). The difference in values using the two routes is within the experimental errors involved, being roughly $\pm 2$ K. The point we wish to emphasize with respect to Table 3 is that in column 6 the $T_g - T_c$ difference was determined using values of $T_g$ obtained via the WLF route and $T_c$ from the dynamic scaling route. On the other hand, the differences as summarized in column 9 were found by using eq 12 to fit for both temperatures together. The agreement between the two methods suggests that the fairly consistent difference between these two temperatures is rather robust and leads us to speculate that we might expect to observe this trend in other miscible blends of flexible polymers.

Figures 6 and 7 provide evidence that the volume associated with a fixed Kuhn length may be used in modeling local compositions so as to predict the distribution of segmental relaxation times, even when density fluctuations are included in an empirical fashion. In particular, a volume as large as the entire cooperative region (which can be 10 times larger than the Kuhn length near $T_g$) is not needed. The physics behind the smaller effective volume is simply that cooperative dynamic events all *start at a small scale* (similar to the Kuhn length). At temperatures close to $T_g$, the cooperative motion has a length scale of order 10 nm for fragile glass-forming liquids, such as flexible polymers.[34,37] But the decision of whether a particular region moves or not is made very locally.[18,32] It is hence the small scales that set the appropriate composition distribution relevant for segmental dynamics.

Having made that point, it is also important to note that our ability to model the composition distribution while making use of only a single fixed length scale (i.e., the Kuhn length) is dependent on our use of a concentration dependence for $T_g$ (and for $T_c$ in the dynamic

scaling model) which is much stronger than that given by the Fox equation. While there is ample precedent for this in the literature, we recognize that the DiMarzio form (eq 2) should be further tested. We plan to do this first by acquiring and analyzing data on blends which show an even larger difference in the component glass transition temperatures than PI and PVE. In addition, a stringent test will be to determine whether our composition dependence will work in the limiting region of dilute composition. We believe that this work provides new pathways for understanding the relaxation behavior of polymer blends and hope that this will spur additional experimental research in this area.

## Appendix

Consider a simple cubic lattice; each site has six nearest neighbors. Suppose that the lattice is completely filled by segments of components polyA and polyB. We shall consider the filling out to the second-neighbor shell of the sites which surround a central site (the "zeroth" shell) occupied by a segment of polyA. The first shell comprises six sites and the second shell an additional 18, for a total of 25 sites.

If we ignore end effects, then the first shell must contain at least two A segments, these being connected to the segment of A in the zeroth shell. There are four sites left in the first shell to be filled. Suppose that the probability of finding a segment of type B in any given site which is a neighbor of a site already filled with an A segment is given by "$p$". The probability of a site next to an A-neighbor being filled by an A segment is therefore $(1 - p)$. Each of the four available sites is filled independently, and so we have the following scenarios:

| free sites with A | free sites with B | probability of filling | total A | total B |
|-------------------|-------------------|------------------------|---------|---------|
| 4 | 0 | $(1-p)^4$ | 6 | 0 |
| 3 | 1 | $4(1-p)^3 p$ | 5 | 1 |
| 2 | 2 | $6(1-p)^2 p^2$ | 4 | 2 |
| 1 | 3 | $4(1-p)p^3$ | 3 | 3 |
| 0 | 4 | $p^4$ | 2 | 4 |

The coefficients in front of the probability results reflect the indistinguishability of the A segments and of the B segments and are just the binomial coefficients. So, for example, with 4 free sites available to fill with 1A and 3B's, there are 4 places for the A and then $3 \times 2 \times 1$

places for the B's; however, the A's and B's are indistinguishable, so the total number of ways of filling the sites is just $(4!/3!1!) = 4$.

The overall distribution is generated by considering, successively, each of the first shell scenarios in filling the second shell and then combining the results. We shall work through one example here:

Consider the case in which there are 4A's and 2B's in the first shell. The probability of this filling is given by $6p^2(1 - p)^2$. There are 18 sites in the second shell. Now, 2 of the 4 A's in the first shell must be bonded to the A segment in the zeroth shell. Therefore, each of these 2 A's in the first shell has one covalent bond to an A in the second shell. The remaining 2 A's in the first shell were not connected to the A in the zeroth shell. They cannot be bonded to each other because they, themselves, are not nearest-neighbors. Therefore, *each* of these 2 A's must be bonded to 2 A's in the second shell. Therefore, there are at least 6 A segments in the second shell, bonded to existing first shell A segments. Similarly, there are 2 B segments in the first shell, and each of these must be bonded to 2 B's in the second shell. Therefore, with no further consideration, we know that of the 18 second shell sites there are at least 6 A segments and 4 B segments. This leaves 8 sites left to fill. In the model which we use here the occupancy of lattice sites, once connectivity requirements have been satisfied, depends only on the site fraction of each component. However, we wish to keep the model general enough that in the future, for strongly interacting blends, we shall have the option of having the nearest-neighbor occupancy depend on nearest-neighbor interactions. Therefore, we frame the rest of the problem by considering the occupancy of the remaining second shell sites to be controlled by their first shell neighbors. We simplify this by assigning each of the 6 first shell sites control over 3 second shell sites.

In the first shell there are 2 A segments which each have only 1 nonbonded second shell neighbor, and there are 2 A segments which have 2 nonbonded second shell neighbors. Therefore, the filling of 6 sites in the second shell is controlled by first shell A segments. Here are the possible filling scenarios, with the associated weighted probabilities (using the binomial coefficients):

|  |  |
|---|---|
| 6 A/0B | $(1 - p)^6$ |
| 5 A/1 B | $6 p(1 - p)^5$ |
| 4 A/2 B | $15 p^2 (1 - p)^4$ |
| 3 A/3 B | $20 p^3(1 - p)^3$ |
| 2 A/4 B | $15 p^4(1 - p)^2$ |
| 1 A/5 B | $6 p^5(1 - p)$ |
| 0 A/6 B | $p^6$ |

Filling of the two remaining sites in the second shell is controlled by first shell B segments. Once again, to obtain the most general results, consider the probability of a site next to a B segment to be filled by an A segment to be given by "$q$"; the probability of that site being filled by a B segment is therefore $(1 - q)$. Thus, for the 2 sites controlled by B segments in the first shell, the weighted filling probabilities are

|  |  |
|---|---|
| 2 B/0 A | $(1 - q)^2$ |
| 1 B/1 A | $2 q(1 - q)$ |
| 0 B/2 A | $q^2$ |

To generate the whole range of possible fillings of the 25 sites *for the particular case of the first shell having 4A and 2B segments,* it remains to multiply together

the probability of finding the first shell with the 4A/2B filling times the probabilities associated with the various filling scenarios for the 8 nonbonded second shell sites. The following set of possibilities are the result, with the total number of A/B segments (zeroth, first, and second shells) given on the left:

|  |  |
|---|---|
| 19A/6B | $6 p^2(1 - p)^8 q^2$ |
| 18A/7B | $12 p^2(1 - p)^8 q (1 - q) + 36 p^3(1 - p)^7 q^2$ |
| 17A/8B | $6 p^2(1 - p)^8 (1 - q)^2 + 72 p^3(1 - p)^7 q (1 - q) +$ <br> $90 p^4(1 - p)^6 q^2$ |
| 16A/9B | $36 p^3(1 - p)^7(1 - q)^2 + 180 p^4(1 - p)^6 q (1 - q) +$ <br> $120 p^5(1 - p)^5 q^2$ |
| 15A/10B | $90 p^4(1 - p)^6 (1 - q)^2 + 240 p^5(1 - p)^5 q (1 - q) +$ <br> $90 p^6(1 - p)^4 q^2$ |
| 14A/11B | $120 p^5(1 - p)^5(1 - q)^2 + 180 p^6(1 - p)^4 q (1 - q) +$ <br> $36 p^7(1 - p)^3 q^2$ |
| 13A/12B | $90 p^6(1 - p)^4(1 - q)^2 + 72 p^7(1 - p)^3 q (1 - q) +$ <br> $6 p^8(1 - p)^2 q^2$ |
| 12A/13B | $36p^7(1 - p)^3(1 - q)^2 + 12p^8(1 - p)^2 q (1 - q)$ |
| 11A/14B | $6p^8(1 - p)^2(1 - q)^2$ |

Sets of probabilities analogous to the above but with differing numbers of A segments and B segments (ranging from 25A/0B to 5A/20B) are generated, corresponding to each of the first shell scenarios. Then, all the terms associated with a given composition are summed, and the result is a complete set of probabilities for each possible filling of the sites, in terms of $p$, $(1 - p)$, $q$, and $(1 - q)$.

In this paper we considered the simple random-mixing case, in which the probability of finding a segment of type A in any site is simply $\phi_A$, the bulk site fraction of A on the lattice. So, for example, suppose $\phi_A = 0.7$. Then, $\phi_A = (1 - p) = 0.7$, $p = 0.3$, $q = 0.7$, and $(1 - q) = 0.3$. Note that in this case $\phi_A = (1 - p) = q$ and $1 - \phi_A = (1 - q) = p$. The probability distribution above is plotted for $\phi_A = 0.7 = (1 - p) = q$ as the point up triangles in Figure 2b.

## References and Notes

(1) Colby, R. H. *Polymer* **1989**, *30*, 1275.
(2) Roovers, J.; Toporowski, P. M. *Macromolecules* **1992**, *25*, 1096, 3454.
(3) Wetton, R. E.; MacKnight, W. J.; Fried, J. R.; Karasz, F. E. *Macromolecules* **1978**, *11*, 158.
(4) Alexandrovich, P. S.; Karasz, F. E.; MacKnight, W. J. *J. Macromol. Sci., Phys.* **1980**, *B17*, 501.
(5) Roland, C. M.; Ngai, K. L. *Macromolecules* **1992**, *25*, 363.
(6) Katana, G.; Kremer, F.; Fischer, E. W.; Plaetschke, R. *Macromolecules* **1993**, *26*, 3075.
(7) Zetsche, A.; Fischer, E. W. *Acta Polym.* **1994**, *45*, 168.
(8) Alegria, A.; Colmenero, J.; Ngai, K. L.; Roland, C. M. *Macromolecules* **1994**, *27*, 4486.
(9) Haley, J. C.; Lodge, T. P.; He, Y.; Ediger, M. D.; von Meerwall, E. D.; Mijovic, J. *Macromolecules* **2003**, *36*, 6142.
(10) Pathak, J. A.; Kumar, S. K.; Colby, R. H. *Macromolecules* **2004**, *37*, 6994.
(11) Chung, G. C.; Kornfield, J. A.; Smith, S. D. *Macromolecules* **1994**, *27*, 964, 5729.
(12) Lodge, T. P.; McLeish, T. C. B. *Macromolecules* **2000**, *33*, 5278.
(13) Leroy, E.; Alegria, A.; Colmenero, J. *Macromolecules* **2003**, *36*, 7280.
(14) (a) Kumar, S. K.; Colby, R. H.; Anastasiadis, S. H.; Fytas, G. *J. Chem. Phys.* **1996**, *105*, 3777. (b) Kamath, S.; Colby, R. H.; Kumar, S. K.; Karatasos, K.; Floudas, G.; Fytas, G. *J. Chem. Phys.* **1999**, *111*, 6121.
(15) Salaniwal, S.; Kant, R.; Colby, R. H.; Kumar, S. K. *Macromolecules* **2002**, *35*, 9211.
(16) Kamath, S.; Colby, R. H.; Kumar, S. K. *Macromolecules* **2003**, *36*, 8567.
(17) Guggenheim, E. A. *Mixtures*; Oxford University Press: Clarendon, 1952.
(18) Rubinstein, M.; Colby, R. H. *Polymer Physics*; Oxford University Press: Oxford, 2003.

(19) Adam, G.; Gibbs, J. H. *J. Chem. Phys.* **1965**, *43*, 139.

(20) Matsuoka, S. *Relaxation Phenomena in Polymers*; Hanser: Cincinnati, 1992.

(21) Donth, E. *The Glass Transition: Relaxation Dynamics in Liquids and Disordered Materials*; Springer: New York, 2001.

(22) Arbe, A.; Alegria, A.; Colmenero, J.; Hoffmann, S.; Willner, L.; Richter, D. *Macromolecules* **1999**, *32*, 7572.

(23) Lipson, J. E. G. *Macromol. Theory Simul.* **1998**, 7, 263.

(24) Luettmer-Strathmann, J.; Lipson, J. E. G. *Macromolecules* **1999**, *32*, 1093.

(25) Reference 12 suggests $\phi_{self} = 0.45$ for PI, based on a Kuhn length which is too small. $\phi_{self} = 0.2$ is actually reasonable for all flexible hydrocarbon polymers without bulky side groups.

(26) The sc lattice ($z = 6$) has 25 sites out to the second shell (1 in the zeroth shell, 6 in the first shell, and 18 in the second shell). Five of these are occupied by the chain that owns the zeroth shell, leaving 20 stochastic sites.

(27) Ferry, J. D. *Viscoelastic Properties of Polymers*, 3rd ed.; Wiley: New York, 1980.

(28) DiMarzio, E. A. *Polymer* **1990**, *31*, 2294.

(29) Kant, R.; Kumar, S. K.; Colby, R. H. *Macromolecules* **2003**, *36*, 10087.

(30) Lutz, T. R.; He, Y.; Ediger, M. D.; Cao, H.; Lin, G.; Jones, A. A. *Macromolecules* **2003**, *36*, 1724.

(31) Lutz, T. R.; He, Y.; Ediger, M. D.; Pitsikalis, M.; Hadjichristidis, N. *Macromolecules* **2004**, *37*, 6440.

(32) Colby, R. H. *Phys. Rev. E* **2000**, *61* 1783.

(33) Erwin, B. M.; Colby, R. H. *J. Non-Cryst. Solids* **2002**, *307−310*, 225.

(34) Erwin, B. M.; Kamath, S. Y.; Colby, R. H. *Phys. Rev. Lett.*, submitted.

(35) Kremer, F., Schönhals, A., Eds.; *Broadband Dielectric Spectroscopy*; Springer: New York, 2003.

(36) Alvarez, F.; Alegria, A.; Colmenero, J. *Phys. Rev. B* **1991**, *44*, 7306.

(37) Tracht, U.; Wilhelm, M.; Heuer, A.; Feng, H.; Schmidt-Rohr, K.; Spiess, H. W. *Phys. Rev. Lett.* **1998**, *81*, 2727.